Optimized axial support topologies for thin telescope mirrors

Luc Arnold
Collège de France et Observatoire de la Côte d'Azur
Laboratoire d'Astrophysique Observationnelle
06460 Caussols, France
E-mail: arnold@ocar01.obs-azur.fr

Abstract. Thin and highly flexible telescope mirrors need to be supported carefully to avoid undesirable elastic deformations and a reduction of their optical quality. In this study, a wide variety of support topologies are examined to provide a basic set of optimized point supports for these telescope mirrors. This is carried out for mirrors without a central hole, with circular and annular entrance pupils. Efficient topologies introducing a small amount of zenith-angle-dependent defocusing are also proposed. The number of supporting points ranges between 3 and 36. Optimal forces and locations of point supports are calculated using thin-plate bending theory. Numerical methods include a linear least-squares method for determining the best forces, and a downhill simplex algorithm to optimize the support locations. The robustness of the proposed solutions is tested by simulated annealing. Scaling laws are briefly reviewed, and support efficiencies are given for each optimized topology. Results show that taking into account the central obscuration ratio (annular pupil) and tolerating a homologous (paraboloidal) deformation of the mirror allows an improvement of efficiency of up to 50% over the case of an unobscured pupil where defocus is not permitted. This work includes a study of support efficiencies versus the Poisson's ratio of the mirror material. Wavefront errors are also estimated in the case of a defective cell, to specify tolerances on forces and support locations.

Subject terms: telescope mirror; mirror deformation; elasticity; mirror support; passive support; active optics; optimization.

Optical Engineering 34(2), 567–574 (February 1995).

1 Introduction

Reducing mirror thickness is important in telescope design. It allows lighter optics, thereby reducing the weight and consequently the cost throughout the whole instrument. Thin mirrors also have superior thermal behavior. However, a well-working supporting system, either passive or active, is required to avoid undesirable deflections under gravitational loading. These deflections must be small enough to maintain the required optical quality.

Geometries and forces have been previously calculated for several axial supporting configurations to minimize the variance of the mirror deflection due to uniform loading. This minimization has been carried out by Nelson *et al.*[1] for unobscured pupils. In this paper, we first extend this work to mirrors without a central hole but with a central obscuration providing annular pupils. We then permit a small amount of homologous deformation, which, after refocusing, does not degrade the image quality. As will be shown, this noticeably increases the efficiency of the support.

Several of the proposed topologies allow a grouping of the supporting points in flotation subsupporting systems, also called load spreaders, such as balances or triangles. This allows passive supporting designs, useful for small and medium-size telescopes of the 1-m class, in which active optics is not justified for several practical reasons: limited number of sources (poor sky coverage) for wavefront sensing because of the small primary-mirror diameter; rapid changes of telescope attitude (as in photometric work, supernova surveys); no change of telescope attitude (as in scanning with CCD in time-delay-integration mode); fully automated and low-maintenance telescopes; minimizing the overall cost of the instrument.

The design of an ideal support would allow for numerous factors: a central hole in the primary; corrections for axisymmetric variation of thickness due to the concave optical surface,[2] the lightweight cored mirror structure,[2,3] the effect of shear forces,[2,3] or the shape of the mirror blank (plate or meniscus).[4,5] The following study is limited to mirrors of uniform thickness without a central hole.

Section 2 presents the scaling laws characteristic of mirror bending under gravitational loading. This allows us to define the efficiency of a support, which is the parameter to be optimized to minimize the rms of the mirror deflection. In Sec. 3, we examine the theoretical problem of support optimization and describe the numerical methods we have used. Section 4 presents the results and discusses the effect of the permitted homologous deformation. It also includes a study of the effect of a change of mirror material on the proposed support efficiencies. In Sec. 5, we quantify the performance of a defective support to fix the tolerances on support locations and forces.

Paper 20064 received June 21, 1994; accepted for publication Sep. 14, 1994.

2 Scaling Laws

By modeling the mirror as a circular thin plate of uniform thickness and describing its deformations under gravitational loading by pure bending theory,[4] we obtain the well-known scaling law[1,6]

$$\delta_{\mathrm{rms}} = \frac{k_{\mathrm{rms}} q a^4}{D} \propto \frac{a^4}{h^2} \ , \tag{1}$$

where δ_{rms} is the rms deflection, q the external load per surface area, a the plate radius, h the plate thickness, and D the flexural rigidity

$$D = \frac{Eh^3}{12(1-\nu^2)} \ . \tag{2}$$

Here E and ν are the material's elastic (Young's) modulus and Poisson's ratio, respectively. The coefficient k_{rms} depends on the support geometry and support forces. A more general form of this law for noncircular plates is given by[1]

$$\delta_{\mathrm{rms}} = \frac{\xi_{\mathrm{rms}} q A^2}{D} \propto \frac{A^2}{h^2} \ , \tag{3}$$

where A is the plate area, and ξ_{rms} is a dimensionless number called the support efficiency that depends on the plate shape and, like k_{rms}, on the support configuration and support forces. The efficiency in terms of peak-to-valley errors, ξ_{ptv}, can be defined in the same manner. Note also that ξ and k depend smoothly on ν, a characteristic of the mirror substrate. Table 1 summarizes the most useful parameters of standard mirror materials. Thus Eqs. (1) and (3) show that, for a given topology and a given mirror, the deflections δ_{rms} and δ_{ptv} can be approximated. We note that, the lower the efficiency ξ, the better the support.

For the optimum method of filling the area under the mirror with supporting points to limit the deflection under gravitational loading, we consider the five two-dimensional Bravais crystal lattices. These describe the five basic geometries of a natural 2-D crystal: oblique, square, rectangular, centered rectangular, and hexagonal lattices. The hexagonal lattice is a grid of adjacent equilateral triangles.[7] It is easy to see that this lattice provides the highest density of nodes per unit area for a given length of the lattice parameters: its density is equal to $2/(u^2\sqrt{3})$, where u is the distance between two nodes. Therefore, the triangular arrangement of supporting points using the hexagonal lattice will provide the most efficient support for an infinite plate. The rms of the deflection is then[1]

$$\delta_{\mathrm{rms}} = 0.00090 \frac{q u^4}{D} \ , \tag{4}$$

and the peak-to-valley amplitude, adapted from Ref. 8, is

$$\delta_{\mathrm{ptv}} = \frac{3}{768} \frac{q u^4}{D} \ . \tag{5}$$

Here, the numerical coefficients do not depend on ν. It is evident therefore that for finite circular plates, it will be reasonable to choose *a priori* a hexagonal lattice for point arrangement and then adjust it to minimize the edge effects.

Table 1 Mechanical properties for mirror blank materials, adapted and extended from the ESO VLT proposal.[12] Materials with asterisks are polycrystalline pure metals.

Material	Specific Mass	Young's Modulus	Poisson's Ratio
		E	ν
	(kg/m^3)	(GPa)	
Aluminium*	2700	70.6	0.345
Titanium*	4500	120.2	0.361
Steel 13/4	7750	210	0.28
Invar	8130	145	0.30
Borosilicate	2230	68	0.20
Ordinary Crown	2500	66.4	0.225
Fused Silica	2202	74.5	0.17
ULE Titanium Silicate	2205	67.6	0.17
Zerodur	2530	91	0.24
CFRP (UHM-quasi-isotropic)	1800	105	0.32

Some useful scaling laws concerning the extra deflection due to shear forces are given by Nelson *et al.*[1] and Wan *et al.*[2] The results presented below do not include the effect of shear. We assume therefore that the mirror thickness is always smaller than the value of the typical distance u between the N supporting points, defined by

$$N\pi u^2 = A \ . \tag{6}$$

3 Optimization and Methods

Our task consists in minimizing the variance δ^2_{rms} of the deflection w over the pupil area S:

$$\delta^2_{\mathrm{rms}} = \int\int_S (w - p_0)^2 \, \mathrm{d}S \ . \tag{7}$$

The term p_0 is a piston term representing the mean value of the deflection. For each support configuration, we optimize forces and locations for the N supporting points. This yields $3N-4$ parameters that should be optimized. Fortunately, this large number can be reduced by adding symmetry conditions on the points' locations. For example, in the three-point support case, points are placed on the same ring, in a three-fold symmetry, and only the supporting radius is optimized.

For larger N, points are initially placed fitting a hexagonal lattice under the mirror. Then the method is the following: points are first grouped in sets of $3n$ having a $3n$-fold symmetry, n being an integer equal to 1 or 2 to fit the hexagonal lattice symmetries. The deflection over the pupil is then computed for each set, and the fraction of mirror weight that each carries is optimized by a least-squares method. This gives a unique solution to minimize δ_{rms}, with the constraint that the total loading of the support must equal the mirror weight. If we denote by η_j the fractional load carried by ring j, the equation (7) can be written

$$\delta^2_{\mathrm{rms}} = \int\int_S \left(\sum_{j=1}^{J} \eta_j w_j - p_0 \right)^2 \mathrm{d}S \ . \tag{8}$$

The constraint is therefore

$$\sum_{j=1}^{J} \eta_j = 1 \ . \tag{9}$$

Taking the derivative of Eq. (8) with respect to all η_j and p_0 provides a set of $J+1$ linear equations. The constraint (9) shows that the variables η_j are not independent, so a Lagrange multiplier method is used to include Eq. (9) in the computation.[9] Then the constraint (9) can be added to the $J+1$ equations as a $(J+2)$'th equation. We thus obtain a linear system of $J+2$ equations to be solved for the $J+2$ unknowns η_j, p_0, and λ, where λ is the Lagrange multiplier. Except if the task is to support an optical flat, a homologous deformation, inducing a small change of focal length, can be easily balanced by refocusing. Therefore the expression to minimize becomes

$$\delta^2_{\text{rms}} = \int\int_S \left(\sum_{j=1}^{J} \eta_j w_j - p_0 - p_2 \rho^2 \right)^2 \, dS \ , \tag{10}$$

where ρ is the radial coordinate in the mirror plane (Fig. 1). The parameter p_2 represents the paraboloidal deformation. Note that p_2 is scaled exactly as δ_{rms} and δ_{ptv} and we can define ξ_{p2} by

$$p_2 = \frac{\xi_{p_2} q A^2}{D} \ . \tag{11}$$

Taking the derivative of Eq. (10) with respect to all η_j, p_0, and p_2 and adding the constraint (9) leads to a linear system of $J+3$ equations with $J+3$ unknowns η_j, p_0, p_2, and λ. The system is solved by singular-value decomposition,[10] which permits control of the numerical stability of the linear system. When the optimal forces and δ_{rms} are computed, the process is iterated: a downhill simplex algorithm[10] chooses new positions (radii and aximuths) for each set of points, and optimal forces are calculated again until the smallest rms is found. Simulated annealing with a small temperature decrease serves to test if the minimum is global. Note that even with slow annealing, one cannot be sure to have found the global minimum and the best support configuration. Nevertheless, our results are encouraging in that several runs with different temperature schedules converge towards the same result.

The mirror surface shape was computed by using a series expansion[1] truncated after 15 terms. The mirror surface was sampled with 28,800 points (288×100, angular and radial direction, respectively), and the Poisson's ratio was fixed at $\nu = 0.24$, corresponding to Zerodur.

4 Results and Discussion

We give here the support efficiencies for configurations with $N=3$ to $N=36$ (Fig. 1). They can be used for an active support, where each point applies a force under the mirror computed by the control loop for the mirror surface. Most of the proposed topologies also allow a flotation (passive) support design, including balances and triangles working as load spreaders. In this last case, the mirror cell will consist of one flotation stage with $N=6$ or 9. It is arranged in two stages with $N=12=3\times(2\times2)$, $N=18=3\times(2\times3)$, or $N=27=3\times(3\times3)$ and three stages when $N=36=3\times[2\times(2\times3)]$. With several flotation stages, the support must be very smooth for a correct force transmission from one stage to the next. The system must also present good damping behavior against vibrations.

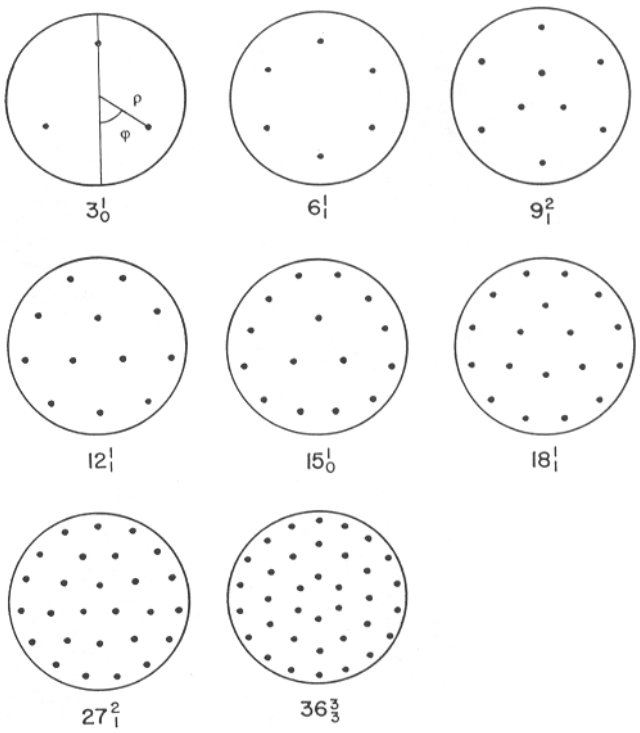

Fig. 1 Optimized topologies, from 3-point to 36-point (adapted from Ref. 1). Here ρ and ϕ are the polar coordinates across the mirror.

The proposed topologies for circular or annular pupils, with or without allowing defocus, are the same as those found by Nelson *et al.*[1] for circular pupils with supports optimized with respect to the mirror plane, except for the 36-point support, for which we found a slightly better configuration very close to a hexagonal lattice. Our results thus concern, using Nelson's notation, the topologies 3_0^1, 6_1^1, 9_1^2, 12_1^1, 15_0^1, 18_1^1, 27_1^2, and 36_3^3. Figure 2 represents the results for the 36_3^3 topology optimized according to different criteria discussed below.

In a telescope, the secondary mirror usually vignettes the central zone of the primary, and it is therefore not necessary to minimize the mirror deflection in this zone. Results for perfect support of unobscured and annular pupils are given in Tables 2 and 3. In the case of $N=3$ and 6, Fig. 3 shows the optimized radius versus the central obscuration ratio (COR). The improvements of ξ are shown in Fig. 4. For a typical COR of 0.3, the improvement of ξ_{rms} rises 10% for $N=18$ and a few percent in other cases. These are rather small and related to the small ratio (9%) of shadowed surface when COR = 0.3. Nevertheless, the positions and forces change noticeably with respect to the unobscured pupil case. Moreover, for Ritchey-Chrétien or Baker-Schmidt telescopes, the COR can reach 0.5, and (as shown in Fig. 4 for $N=6$) ξ_{rms} could be improved by 28%. As pointed out in the introduction, the effect of a possible central hole should be taken into account.

If a small amount of defocus over the mirror is tolerated, Tables 4 and 5 show that ξ_{rms} can be improved by 20 to 40%, depending on the configuration. The small change in focal length is not static, but depends on the zenith angle z, being proportional to cos$z$. The variation ε of focal length is given by

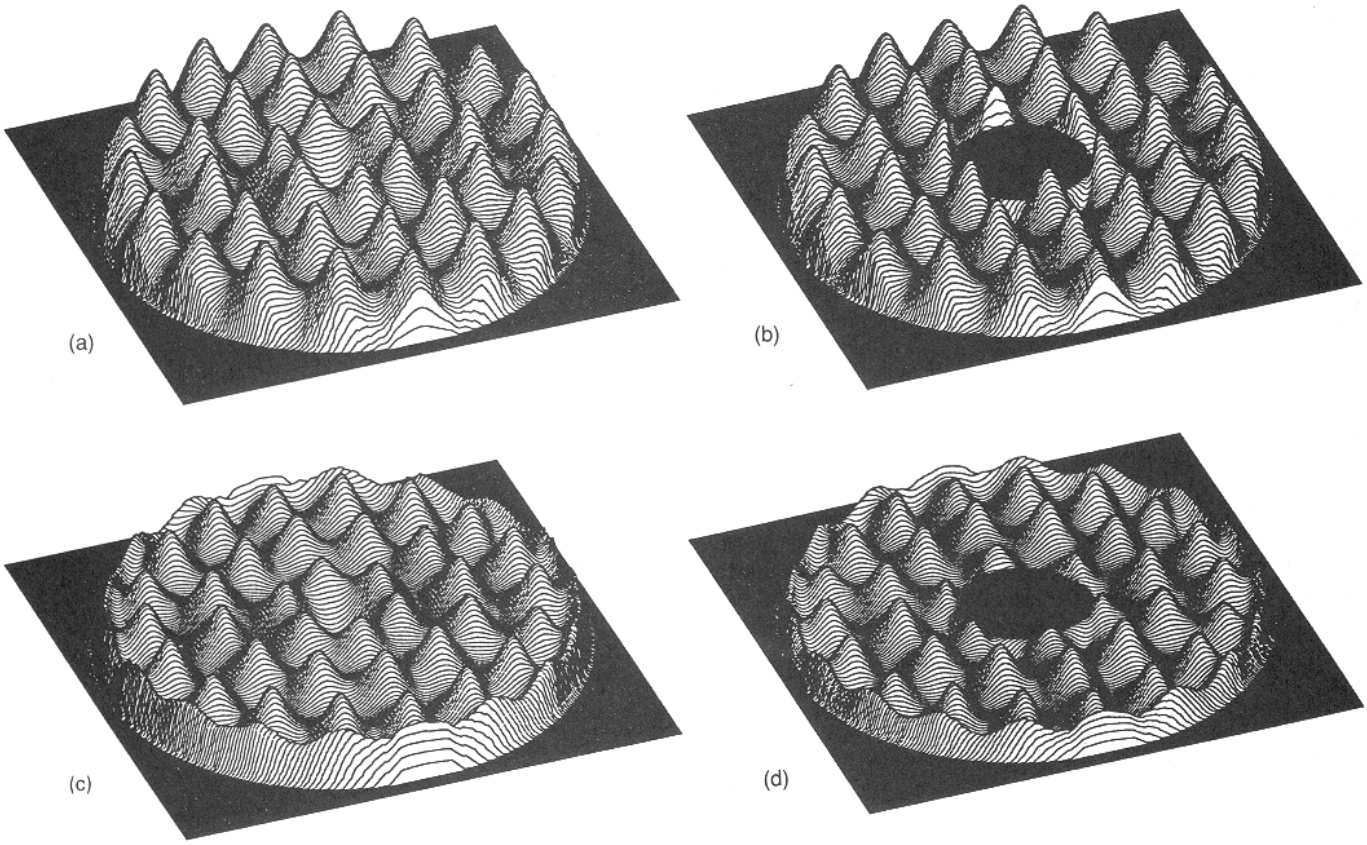

Fig. 2 Mirror shapes for the 36-point support represented with a constant vertical scale: (a) optimization for unobscured pupil with respect to the mirror plane; (b) optimization for annular pupil (COR = 0.3) with respect to the mirror plane; (c) optimization for unobscured pupil with respect to the nearest paraboloid; (d) optimization for annular pupil (COR = 0.3) with respect to the nearest paraboloid.

Table 2 Optimized topologies for unobscured pupil: central obscuration ratio = 0.0. No defocus is tolerated. Poisson's ratio is set at $\nu = 0.24$; n_j is the number of points on ring i; η_i, ρ_i, and ϕ_i have been optimized, and integer values of ϕ_i have been fixed.

N	$\xi_{ptv}.10^5$	$\xi_{rms}.10^5$	n_i,	$\rho_i.10^4$,		$\eta_i.10^4$,		ϕ_i (deg)				
3	264	59.2	ρ=6454									
6	35.6	8.04	ρ=6811									
9	23.0	4.54	n=3	3		3						
			ρ=2896	7973		7708						
			η=2369	3586		4045						
			ϕ=0	0.00		60.00						
12	7.44	1.34	n=3	3		3		3				
			ρ=3141	7660		8244		8244				
			η=2767	2838		2198		2198				
			ϕ=0	60		20.06		-20.06				
15	5.71	1.02	n=3	3		3		3		3		
			ρ=3178	7758		7758		8397		8397		
			η=2811	2049		2049		1546		1546		
			ϕ=0	44.87		-44.87		14.97		-14.97		
18	3.33	0.567	n=3	3		3		3		3	3	
			ρ=4686	3194		8166		8166		8503	8503	
			η=1599	2053		1732		1732		1442	1442	
			ϕ=0	60		44.80		-44.80		15.24	-15.24	
27	1.30	0.217	n=3	3		3		3		3	3	3	3
			ρ=2101	8637		4800		5556		5556	8847	8847	8564	8564
			η=1188	1087		1291		1167		1167	920	920	1130	1130
			ϕ=0	0		60		20.38		-20.38	24.15	-24.15	47.83	-47.83
36	0.709	0.125	n=6	6		6		6		6	6			
			ρ=2548	5590		5904		8906		8777	8777			
			η=1643	1847		1772		1458		1641	1641			
			ϕ=0	30		0		0		19.87	-19.87			

Table 3 Optimized topologies for annular pupil: central obscuration ratio = 0.3. No defocus is tolerated. Poisson's ratio is set at $\nu = 0.24$; n_j is the number of points on ring i; η_i, ρ_i, and ϕ_i have been optimized, and integer values of ϕ_i have been fixed.

N	$\xi_{ptv}.10^5$	$\xi_{rms}.10^5$	n_i,	$\rho_i.10^4$,		$\eta_i.10^4$,		ϕ_i (deg)				
3	256	60.1	ρ=6379									
6	29.6	6.62	ρ=6861									
9	22.9	4.75	n=3	3		3						
			ρ=3302	8081		7687						
			η=2565	3378		4057						
			ϕ=0	0.00		60.00						
12	7.25	1.32	n=3	3		3		3				
			ρ=2661	7774		8116		8116				
			η=2576	2727		2348		2348				
			ϕ=0	60		20.02		-20.02				
15	6.30	0.961	n=3	3		3		3		3		
			ρ=2704	7836		7836		8209		8209		
			η=2615	2000		2000		1693		1693		
			ϕ=0	44.91		-44.91		14.95		-14.95		
18	2.62	0.494	n=3	3		3		3		3	3	
			ρ=4079	4079		8407		8407		8407	8407	
			η=1949	1949		1526		1526		1526	1526	
			ϕ=0	60		44.78		-44.78		15.22	-15.22	
27	1.18	0.207	n=3	3		3		3		3	3	3	3	3
			ρ=1736	8639		5245		5587		5587	8851	8851	8653	8653
			η=1270	1085		1240		1222		1222	911	911	1069	1069
			ϕ=0	0		60		20.62		-20.62	24.14	-24.14	47.70	-47.70
36	0.620	0.110	n=6	6		6		6		6	6			
			ρ=3080	5817		6343		9047		8827	8827			
			η=2114	1780		1654		1286		1583	1583			
			ϕ=0	30		0		0		19.83	-19.83			

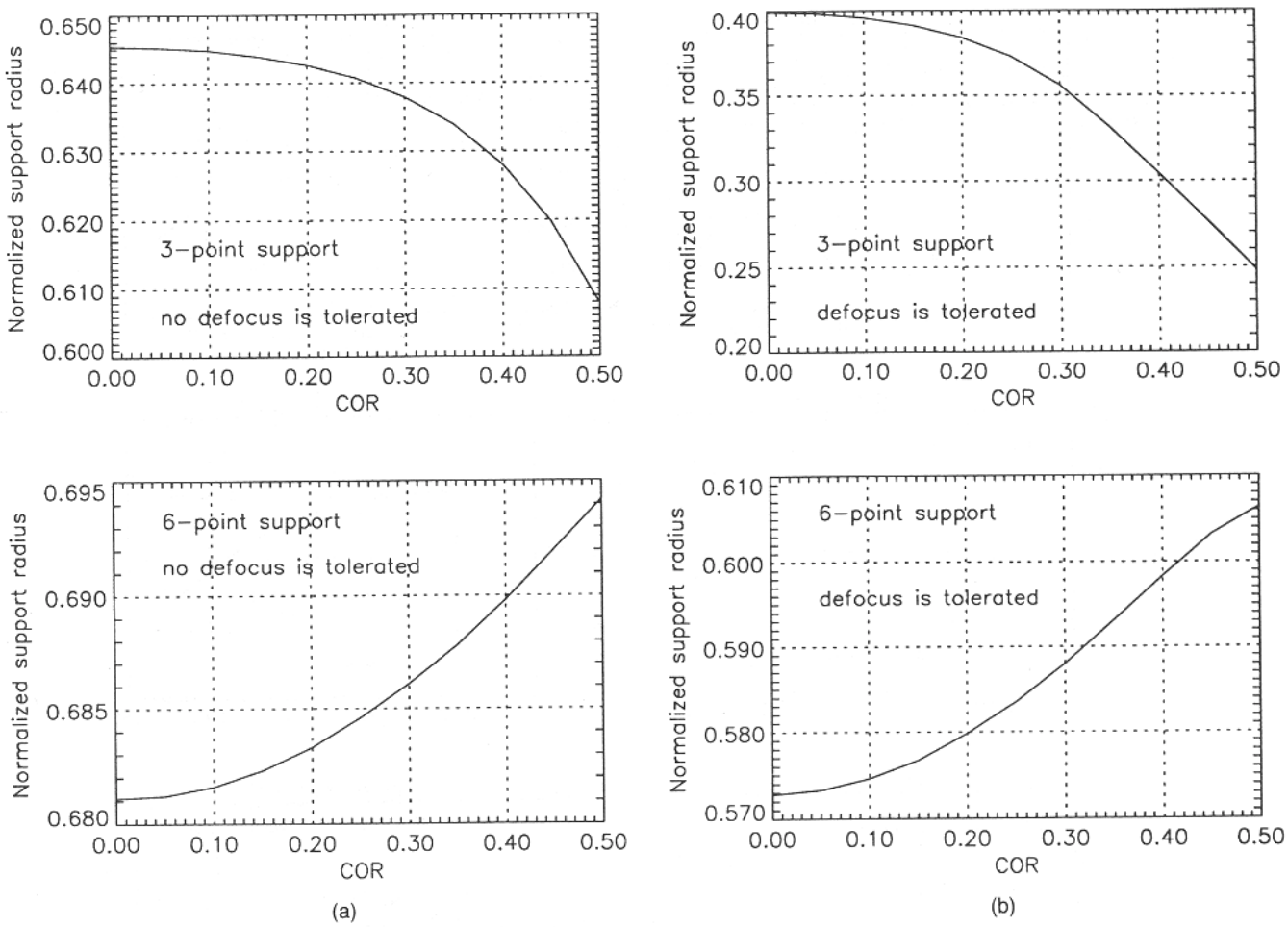

Fig. 3 Optimized support radii ρ for the three-point and six-point supports versus central obscuration ratio (COR). The rms deflection is minimized with respect to the mirror plane (a) or to the nearest paraboloid (b).

$$\varepsilon = 16\left(\frac{f}{D_t}\right)^2 p_2(1-\cos z) \ , \tag{12}$$

or, with Eq. (11) corresponding to the thin-plate mirror model,

$$\varepsilon = 16\left(\frac{f}{D_t}\right)^2 \frac{\xi_{p_2} q A^2}{D}(1-\cos z) \ , \tag{13}$$

where f is the focal length and D_t the telescope diameter.

Let us consider, as an example, a 30-mm-thick, 600-mm-diam borosilicate mirror. With a focal ratio of 5, this primary can be combined with two different secondary mirrors in two *f*/15 Cassegrain or *f*/30 Coudé-Cassegrain configurations. We assume the mirror is horizontal and supported by a perfect nine-point system optimized for an unobscured pupil. This leads to 90-nm peak-to-valley and 19-nm rms wavefront errors after refocusing. The parameter ξ_{p_2} is equal to 175×10^{-5} and induces, at $z = 60$ deg, focus changes of $\varepsilon \approx 1.0$ mm and $\varepsilon \approx 4.1$ mm, respectively. If this defocus is not corrected, the Strehl ratio decreases to ≈77% and ≈1%, respectively, when other sources of aberrations, including seeing effects, are neglected.[11] Fortunately, focusing routines are usually provided on telescopes to balance the change of focal length brought about by thermal effects. Note also that if the defocus induced by ξ_2 is considered too large, ξ_2 can be fixed at an intermediate value fulfilling the specifications, and the support reoptimized. This leads to intermediate values of ξ_{rms} and ξ_{ptv}.

A by-product of the better efficiency obtained with a mirror cell incorporating correctable defocus is a reduction in the scalloping of the mirror surface. Thus, larger telescopes having active and adaptive systems, and thus diffraction limited, will have a point spread function where the first diffraction ring will not be segmented, nor modulated in brightness. This is useful from an astrophysical point of view, when methods involving deconvolution are used to study stellar rings or diffuse shells.

As pointed out in Sec. 2, the efficiencies ξ depend smoothly on the Poisson's ratio ν. The previously optimized configurations from Table 2 for Zerodur ($\nu = 0.24$) were used to calculate the relative variation of efficiency, $\Delta(\xi_{\text{rms}})$, given by

$$\Delta(\xi_{\text{rms}}) = 100 \times \frac{\xi_{\text{rms}}(\nu) - \xi_{\text{rms}}(\text{Zerodur})}{\xi_{\text{rms}}(\text{Zerodur})} \tag{14}$$

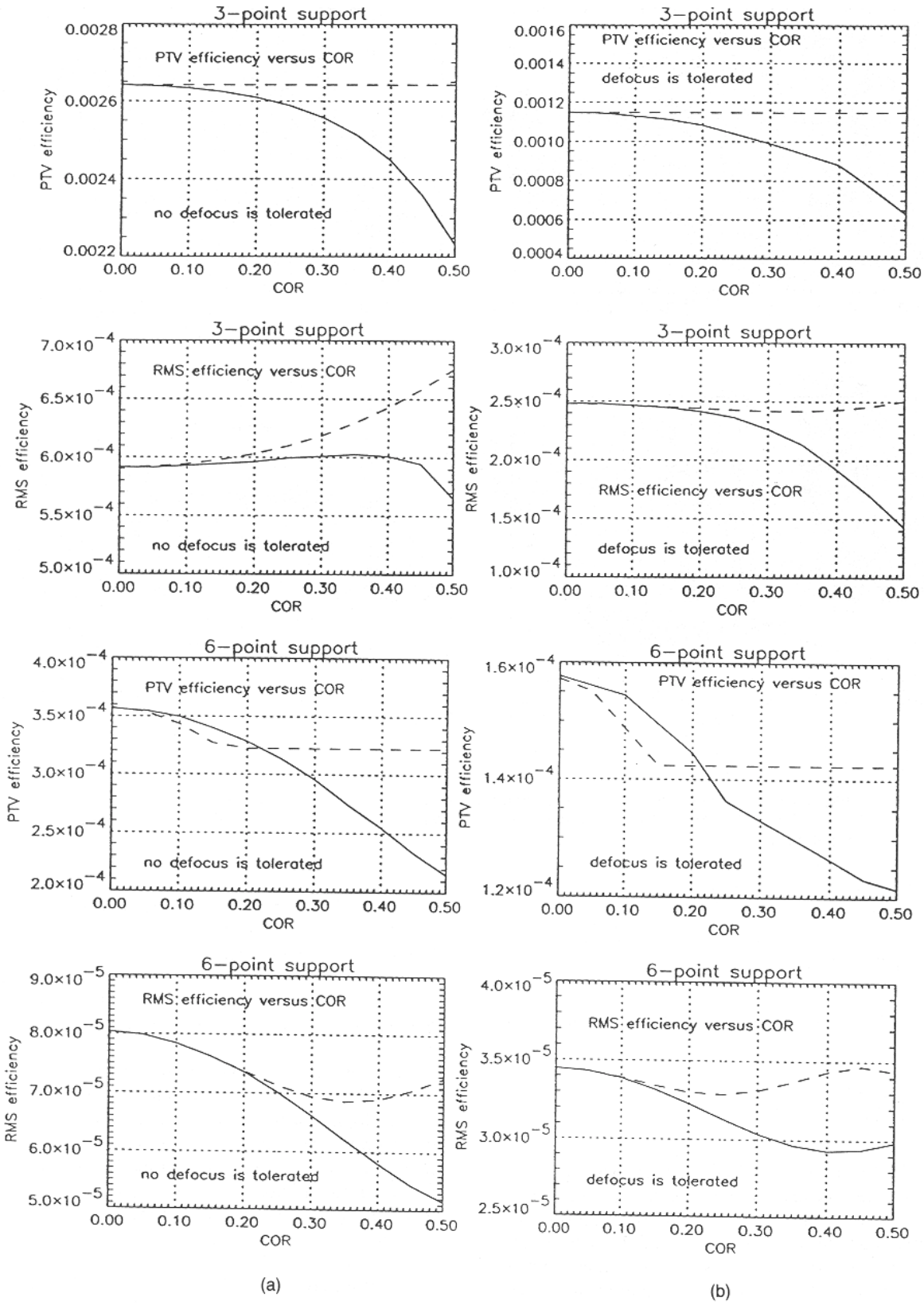

Fig. 4 Three-point and six-point support efficiencies versus central obscuration ratio (COR). The rms deflection is minimized with respect to the mirror plane (a) or to the nearest paraboloid (b). The dashed line represents the efficiency over an annular pupil when the support has been optimized over an unobscured pupil. The solid line represents the improvement of the efficiency over an annular pupil when the support has been optimized over the same annular pupil.

Table 4 Optimized topologies for unobscured pupil: central obscuration ratio = 0.0. Defocus is tolerated. Poisson's ratio is set at $\nu = 0.24$; n_i is the number of points on ring i; η_i, ρ_i, and ϕ_i have been optimized, and integer values of ϕ_i have been fixed.

N	$\xi_{ptv}.10^5$	$\xi_{rms}.10^5$	$\xi_{p-v}.10^5$	n_i,	$\rho_i.10^4$,	$\eta_i.10^4$,	ϕ_i (deg)					
3	115	24.8	539	ρ=3991								
6	15.8	3.45	224	ρ=5729								
9	13.6	2.79	175	n=3	3	3						
				ρ=1475	6345	6328						
				η=1014	4470	4517						
				ϕ=0	0.00	60.00						
12	4.48	0.840	105	n=3	3	3	3					
				ρ=2626	6905	7148	7148					
				η=1995	2899	2553	2553					
				ϕ=0	60	20.06	-20.06					
15	3.33	0.600	96.3	n=3	3	3	3	3				
				ρ=2709	7017	7017	7296	7296				
				η=2098	2118	2118	1833	1833				
				ϕ=0	45.00	-45.00	15.05	-15.05				
18	1.91	0.373	76.5	n=3	3	3	3	3	3			
				ρ=4004	2894	7448	7448	7576	7576			
				η=1222	1612	1863	1863	1720	1720			
				ϕ=0	60	44.94	-44.94	15.16	-15.16			
27	0.816	0.161	47.3	n=3	3	3	3	3	3	3	3	3
				ρ=1895	7989	4426	5013	5013	8075	8075	7956	7956
				η=968	1234	1097	967	967	1130	1130	1254	1254
				ϕ=0	0	60	20.32	-20.32	24.13	-24.13	47.91	-47.91
36	0.564	0.0958	37.1	n=6	6	6	6	6	6			
				ρ=2352	5202	5403	8259	8214	8214			
				η=1390	1589	1534	1759	1864	1864			
				ϕ=0	30	0	0	19.91	-19.91			

Table 5 Optimized topologies for annular pupil: central obscuration ratio = 0.3. Defocus is tolerated. Poisson's ratio is set at $\nu = 0.24$; n_i is the number of points on ring i; η_i, ρ_i, and ϕ_i have been optimized, and integer values of ϕ_i have been fixed.

N	$\xi_{ptv}.10^5$	$\xi_{rms}.10^5$	$\xi_{p-v}.10^5$	n_i,	$\rho_i.10^4$,	$\eta_i.10^4$,	ϕ_i (deg)					
3	97.2	22.7	577	ρ=3560								
6	13.2	3.04	198	ρ=5881								
9	13.5	2.90	177	n=3	3	3						
				ρ=3093	6386	6251						
				η=1236	4177	4587						
				ϕ=0	0.00	60.00						
12	4.09	0.819	101	n=3	3	3	3					
				ρ=2005	7023	7128	7128					
				η=1884	2805	2656	2656					
				ϕ=0	60	20.02	-20.02					
15	3.07	0.519	91.7	n=3	3	3	3	3				
				ρ=2064	7124	7124	7244	7244				
				η=1970	2069	2069	1946	1946				
				ϕ=0	45.00	-45.00	15.01	-15.01				
18	1.56	0.336	66.0	n=3	3	3	3	3	3			
				ρ=3700	3700	7650	7650	7650	7650			
				η=1586	1586	1707	1707	1707	1707			
				ϕ=0	60	44.85	-44.85	15.15	-15.15			
27	0.753	0.157	45.0	n=3	3	3	3	3	3	3	3	3
				ρ=1571	8038	4890	5139	5139	8137	8137	8051	8051
				η=1073	1212	1069	1042	1042	1090	1090	1191	1191
				ϕ=0	0	60	20.55	-20.55	24.13	-24.13	47.80	-47.80
36	0.437	0.0894	33.5	n=6	6	6	6	6	6			
				ρ=2837	5456	5825	8403	8316	8316			
				η=1786	1589	1474	1595	1778	1778			
				ϕ=0	30	0	0	19.87	-19.87			

as a percentage versus ν, ranging between fused silica ($\nu = 0.17$) and titanium ($\nu = 0.361$, Table 1). This was done initially without readjusting the forces, although that should further decrease the variation of ξ_{rms}. Figure 5 represents $\Delta(\xi_{rms})$ for the 36-point support, for which the effect is the largest. It shows that the variation of efficiency is quite small, typically $\approx 5\%$. A loss of efficiency is observed for $\nu \neq 0.24$. Deformations are mostly defocus and spherical aberrations. Nevertheless, $\Delta(\xi_{rms})$ remains small, and (with the exception of titanium, which is the extreme case) the proposed support topologies do not need to be reconsidered.

5 Tolerance Analysis

It is important in practice to know the tolerance on the points' locations and forces for use in mechanical specifications. This can be estimated by a simple model where the positions and forces of the N supporting points are perturbed. Ideally, position and force would be perturbed independently for each supporting point, with the exception of three points for which forces should be constrainted to maintain static equilibrium. In our model, points are grouped in sets of two or three, and the center of symmetry of a pair or a triplet of points corresponds to the mirror center. This arrangement allows the use of a series expansion for each elementary set (see Sec. 3). The radius ρ, the azimuthal position ϕ under the mirror, and the carried load η are perturbed for each set of points, and the deflection computed. The global deflection is then derived by superimposing the contributions of all groups. The three perturbations follow a Gaussian probability law. The standard deviations for ρ and ϕ are related to σ_x and σ_y, the standard deviations for the points' locations in the mirror plane in Cartesian coordinates. As no net moment is applied by the perturbed doublets or triplets, only the force η for the final randomly chosen set has to balance the mirror weight. The model is best applied when the points are grouped by pairs rather than by triplets. We therefore slightly modified the previously studied topologies to allow this arrangement. For example, we reoptimized the 18-point support in a new configuration with three rings of six points. The efficiencies for these new supports were very similar to the real optimal ones.

We carried out two different runs with $\sigma_x = \sigma_y = 0.002$ and $\sigma_x = \sigma_y = 0.005$, with the standard deviation of η equal to zero. We then assumed $\sigma_\eta = 0.001$ and 0.002 for two more simulations, with $\sigma_x = \sigma_y = 0.0$. The mean values of the efficiencies over 100 runs for each perturbed topology are given in Table 6. A Zernike decomposition of the aberrated wavefront mainly shows third-order astigmatism. The value of ξ_{ptv} can be deduced from the relation $\xi_{ptv}/\xi_{rms} \approx 5$, derived from this simulation. The theoretical value of this ratio for pure astigmatism is 4.90. The results show that the efficiency decreases monotonically with increasing number of points when only errors on point positions are present. But when $\sigma_\eta \geq 0.0$, this is no longer true, and the 36-point support seems to be more sensitive to noise on forces than the 27-point support. The efficiency is more sensitive to noise on point forces than on position. To adjust ξ_{rms} to a value close to the optimum, it is necessary to be able to control the points' loading with an accuracy better than 0.1%, or even 0.01% for $N \geq 12$. Of course, this fine tuning can only be done with levers or actuators with load cells. In the case of a simple passive mirror cell with only balances or triangles as load spreaders, the mechanics must be as smooth as possible to allow a good force distribution.

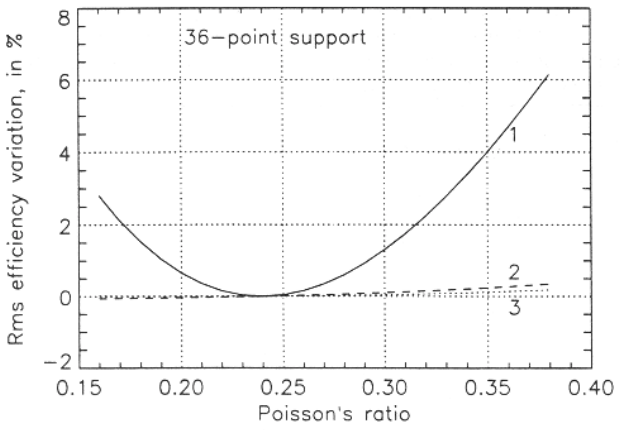

Fig. 5 Variation of 36-point support efficiency $\Delta(\xi_{rms})$ versus Poisson's ratio ν. Curve 1: without removing the defocus of the deformation; curve 2: with defocus removed; curve 3: when forces are reoptimized.

Table 6 Estimated efficiencies ξ_{rms} ($\times 10^5$) after refocusing, for the defective supports of Table 2. Topologies have been slightly modified as explained in Sec. 5. Poisson's ratio is set at $\nu = 0.24$. Standard deviations for the points' location in the mirror plane are σ_x, σ_y, and for the points' loading, σ_η. The value of ξ_{ptv} can be deduced from the relation $\xi_{ptv}/\xi_{rms} \approx 5$, derived from this simulation and indicating the presence of astigmatism.

N	6	9	12	15	18	27	36
$\sigma_{x,y} = 0.0,\ \sigma_\eta = 0.0$	8.04	4.54	1.34	1.02	0.567	0.217	0.125
$\sigma_{x,y} = 0.0,\ \sigma_\eta = 0.001$	8.1	4.8	4.7	2.3	1.9	1.7	2.6
$\sigma_{x,y} = 0.0,\ \sigma_\eta = 0.002$	8.4	5.1	5.2	3.3	3.4	3.2	4.8
$\sigma_{x,y} = 0.002,\ \sigma_\eta = 0.0$	8.3	4.8	4.7	1.8	1.1	0.91	0.63
$\sigma_{x,y} = 0.005,\ \sigma_\eta = 0.0$	9.3	5.9	5.7	3.0	2.2	1.9	1.7

6 Conclusion

The goal of this paper was to study the characteristics of basic axial support topologies for carrying thin and flexible telescope mirrors, based on a thin-plate model with constant thickness under pure bending. We have here extended the previous work by Nelson *et al.*[1] for unobscured entrance pupils and studied several optimized supports, taking into account the central obscuration ratio, and tolerating a small change of focal length induced by the support. We showed that this allows noticeable improvements in efficiencies, of up to 50% over the best efficiencies computed for unobscured pupils without tolerating defocus. We also examined the effect on support efficiency induced by a change of mirror material. Furthermore, we have quantified the performance of defective mirror supports.

Acknowledgments

The author is grateful to the Collège de France, Paris, which funded this work. Constructive comments on the manuscript by Peter Lawson and Antoine Labeyrie are gratefully acknowledged.

References

1. J. E. Nelson, J. Lubliner, and T. S. Mast, "Telescope mirror supports: plate deflection on point supports," in *SPIE Conf. on Advanced Technology Optical Telescopes, Proc. SPIE* **332,** 212–228 (1982).
2. D. S. Wan, J. R. P. Angel, and R. E. Parks, "Mirror deflection on multiple axial supports," *Appl. Opt.* **28**(2), 354–362 (1989).
3. W. P. Barnes, Jr., "Optical design of cored mirror structures," *Appl. Opt.* **8**(6), 1191–1196 (1969).
4. S. Timoshenko, and S. Woinowsky-Krieger, *Theory of Plates and Shells,* 2nd ed., McGraw-Hill, New York (1959).
5. G. Schwesinger, "An analytical determination of the flexure of the 3.5 m primary and 1 m mirror of the ESO's New Technology Telescope for passive support and active control," *J. Modern Opt.* **35**(7), 1117–1149 (1988).
6. A. Couder, *Recherches sur les déformations des Grands Miroirs Employés aux Observations Astronomiques,* PhD, Gauthier-Villars, Paris (1932).
7. C. Kittel, *Introduction to Solid State Physics,* 5th ed., Wiley, New York (1976).
8. G. Lemaitre, "Various aspects of active optics," in *SPIE Conf. on Telescopes and Active Systems, Proc. SPIE* **1114,** 328–350 (1989).
9. G. Arfken, *Mathematical Methods for Physicists,* Academic Press, New York (1966).
10. W. H. Press, S. A. Teukolsky, W. T. Vettering, and B. P. Flannery, *Numerical Recipes in C,* 2nd ed., Cambridge Univ. Press (1992).
11. V. N. Mahajan, "Aberrated point spread functions for rotationally symmetric aberrations," *Appl. Opt.* **22**(19), 3035–3041 (1983).
12. European Southern Observatory, *Proposal for the Construction of the 16–m Very Large Telescope,* ESO, Garching-bei-München (Mar. 1987).

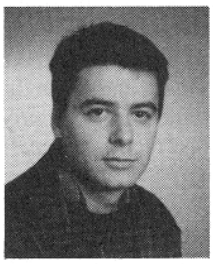

Luc Arnold received a Magistère in materials sciences and a Diplome d'Etudes Approfondies in physical chemistry from Strasbourg-I and Haute Alsace Universities in 1991. He is now with the Laboratoire d'Astrophysique Observationnelle, Collège de France, and Département A. Fresnel, Observatoire de la Côte d'Azur. His thesis, currently in preparation, concerns several aspects of elastic deformations applied to active and adaptive mirrors. He is also contributing to the development of the Optical Very Large Array prototype telescope.